Mechanics of Ultra-Strength Materials

Ting Zhu, Ju Li, Shigenobu Ogata, and Sidney Yip

Abstract

Recent experiments on nanoscale materials, including nanowires, nanopillars, nanoparticles, nanolayers, and nanocrystals, have revealed a host of "ultra-strength" phenomena, defined by stresses in the material generally rising up to a significant fraction of the ideal strength—the highest achievable strength of a defect-free crystal. This article presents an overview of the strength-controlling deformation mechanisms and related mechanics models in ultra-strength nanoscale materials. The critical role of the activation volume is highlighted in understanding the deformation mechanisms, as well as the size, temperature, and strain rate dependence of ultra strength.

Introduction

An engineering revolution is currently under way in that small structures and devices are now being fabricated at the micrometer to nanometer scales. The reliability concerns of such small systems call for an understanding of the mechanical properties of materials at small length scales.[1] This review focuses on the ultra-strength behavior in materials with very small length scales.

Ultra-strength phenomena are characterized by sample-wide stress levels reaching a significant fraction of the material's ideal strength, defined as the highest stress a perfect crystal can sustain without undergoing immediate structural transformation.[2–4] There is an intimate relation between observable strength and the timescale of observation. It is difficult to avoid "observing" ultra strength in molecular dynamics simulations because of the short simulation time scales, typically nanoseconds, for stress ramp-up. But in recent years, more and more ultra-strength behaviors are revealed in laboratory experiments, typically on the seconds-to-minutes time scale. This is often enabled by the small sample sizes, small microstructural length scales, or small probes.

The purpose of this article is to review recent experiments on ultra-strength materials and develop a theoretical framework for understanding the strength-controlling deformation mechanisms. We focus on the ultra-strength phenomena in crystalline materials, while noting that the deformation of amorphous solids often operates at very high stresses; the deformation behavior of metallic glasses has recently been reviewed by Schuh et al.[5]

Ultra-Strength Experiments

Recent years have seen rapid growth of experimental studies on ultra-strength material systems and phenomena. This is largely enabled by the refinement of nanoscale mechanical experiments, which allows one to study the near-ideal-strength behavior quantitatively in a controlled fashion. Table 1 shows the experimentally measured ultra strengths. These data are either yield or fracture strengths measured from tension, compression, or bending experiments. Evidently, ultra-strength behavior can be considered as a GPa-level phenomenon, in contrast to the relatively low strengths (tens to hundreds of MPa) in coarse-grained hard materials. In addition, a collection of ultra-strength data for nanoindentation and nanocrystals can be found in References 6 and 7.

Length-Scale Effect

The attainment of ultra strength can result from a length-scale effect. For coarse-grained crystals, the experimentally measured strengths are far below the theoretical values. The low strength arises because the sample usually has a large number of grown-in defects such as dislocations or cracks. In well-annealed crystals, the dislocation density is initially low but nonzero. It increases rapidly once deformation starts, due to, for example, double cross slip and Frank-Read type multiplication processes. The yield strength is then limited by the resistance to dislocation motion, typically a factor of 100 below the ideal strength, or even more in coarse-grained samples.

The strength of materials with pre-existing defects can be increased by reducing systems' length scales. Gene-

Table I. Experimentally Measured Ultra-High Strengths.

Material	Number of Layers or Diameter (nm)	Measured Strength (GPa)	Ideal Strength ~ *E*/10 (GPa)	Reference
CNT	SW	30	100	Falvo et al.[8]
CNT	MW	30	100	Yu et al.[9]
CNT	MW	97–110	100	Peng et al.[10]
WS_2-NT	MW	3.8–16.3	15	Kaplan-Ashiri et al.[11]
ZnO-NW	30	7	14	Wen et al.[12]
Si-NW	100–200	12	17	Hoffmann et al.[13]
Ag-NW	16.5	7.3	8	Wu et al.[14]
Au-NW	40	5.6	8	Wu et al.[15]
Au-NP	300	0.8	8	Greer and Nix[16]
Au-NP	300	1	8	Volkert et al.[17]
Si-NS	20–50	20–50	17	Gerberich et al.[18]
CdS-NS	200–450	2.2	4.6	Shan et al.[19]
Graphene	ML	130	100	Lee et al.[20]

Note: CNT, carbon nanotubes; NT, nanotubes; NW, nanowires; NP, nanopillars; NS, nanospheres; ML, monolayer; SW, single-wall; MW, multi-wall; *E*, Young's modulus.

rally, the strength-controlling length scale can be the sample size, grain size, layer thickness, or contact loading zone size. In crystals, the strengthening mechanism is typically based on the blockage or elimination of dislocations. Various detailed size-strengthening mechanisms will be reviewed in this article.

Time Scale Effect

Ultra-strength phenomena are also closely related to the observation time scale, as manifested by the dependence of strength on loading rate and temperature. To understand the strength, temperature, and time scale relations, one needs to know the controlling deformation mechanism, which is the focus of this review. Then the kinetic rate theory can be used to link time and strength. Fundamental concepts in the rate theory of strength, with emphasis on the activation volume as a kinetic signature of deformation mechanism, are reviewed next.

A unit process of strength-controlling structural transformation can be characterized by two types of quantitative measures: the athermal strength limit and activation parameters. The former measures the zero-temperature structural stability limit at which the structural transformation occurs instantaneously without the aid of thermal fluctuations. The activation parameters, including the activation energy and activation volume, characterize the probabilistic nature of transformation by thermal fluctuations when the applied load is below the athermal limit. Consider, as an example, thermally activated shear transformation at a given temperature T and applied shear stress τ. According to transition state theory,[21] the transformation rate is

$$\nu = N\nu_0 \exp\left(-\frac{Q(\tau,T)}{k_B T}\right), \quad (1)$$

where ν_0 is the trial frequency, N is the number of equivalent sites of transformation, k_BT is the thermal energy, and Q is the activation free energy whose magnitude is controlled by the local shear stress τ along with the temperature T. The athermal strength limit corresponds to the critical stress, giving zero activation energy.

The sensitivity of transformation rate to stress can be measured by the true activation volume Ω, defined as

$$\Omega = -\frac{\partial Q}{\partial \tau} = k_B T \frac{\partial \ln \nu}{\partial \tau}. \quad (2)$$

Physically, the activation volume is proportional to the number of atoms simultaneously involved in a thermally activated process so that it measures the individual (single-particle) and collective nature of a transition. Different rate processes may have drastically different characteristic activation volumes (e.g., $\Omega \sim 0.1b^3$ for lattice diffusion and $\Omega \sim 100 - 1000b^3$ for Orowan looping through forest dislocation intersections, where **b** denotes the magnitude of the Burgers vector). As a result, the activation volume can serve as an effective kinetic signature of the deformation mechanism.

Importantly, activation volume can be determined by both atomistic modeling and experiments, thus providing a useful link between the two approaches for revealing the strength-controlling mechanisms. In atomistic modeling, the stress-dependent activation energy and activation volume can be calculated in a robust and efficient manner by using the reaction pathway exploration approach such as the nudged elastic band method.[22] In experiments, the activation volume is typically determined by measuring the strain rate sensitivity. Consider uniaxial tension as an example. The empirical power law relation between stress σ and strain rate $\dot{\varepsilon}$ is $\sigma/\sigma_0 = (\dot{\varepsilon}/\dot{\varepsilon}_0)^m$, where m is the nondimensional rate sensitivity index, σ_0 is the reference stress, and $\dot{\varepsilon}_0$ is the reference strain rate. The apparent activation volume Ω^* is conventionally defined as

$$\Omega^* = \sqrt{3}\, k_B T \frac{\partial \ln \dot{\varepsilon}}{\partial \sigma}. \quad (3)$$

This leads to $m = \sqrt{3}\, k_BT/\sigma\Omega^*$. For polycrystals, the true and apparent activation volumes are related by $\Omega^* = \Omega\sqrt{3}/M$, where $M \approx 3.1/A$. Here 3.1 is the Taylor factor that links the tensile flow stress of the polycrystalline aggregate to the average resolved shear stress on the activated slip system, and A is a stress amplification factor (ratio of local shear stress to average resolved shear stress) due to, for example, dislocation pile-up that can be grain or sample size dependent.

Strength-Controlling Deformation Mechanisms

Because of the interposition of small length scales, the deformation of ultra-strength materials often operates in a source-limited and nucleation-controlled regime. We next review representative deformation mechanisms in ultra-strength materials. The critical role of activation volume is emphasized in understanding the strength-controlling mechanisms, as well as the size, temperature, and strain rate dependence of material responses.

Dislocation Nucleation

Ultra strength can be achieved in a small volume of perfect crystal. At low temperatures, the strength of a perfect crystal is limited by dislocation nucleation in the bulk or from the surface, depending on the sample geometry and loading mode. Homogenous dislocation nucleation in the bulk crystal has been experimentally observed in the atomic model systems of bubble raft[23] and colloidal crystal[24] and also in atomistic simulations.[25] In addition, displacement bursts in nanoindentation experiments have been associated arguably with homogeneous dislocation nucleation in a small and perfect volume beneath the nano-sized indenter tip.[25]

Athermal dislocation nucleation in a perfect crystal results from elastic instability at large shear stress; equivalently, it occurs when the energy barrier of nucleation vanishes. Because of the elastic softening effect at large deformation, the athermal threshold of homogeneous dislocation nucleation should be determined by using the theory of hyperelastic (i.e., nonlinear elastic) instability.[26] An atomistics-based hyperelastic instability criterion has been developed that balances the elastically softening modulus and the GPa-level high stress at large shear.[25] Using this criterion, the critical nucleation conditions at zero temperature can be accurately predicted, including the nucleation site, critical stress, and activated slip system. The athermal nucleation from a surface can be similarly modeled in the hyperelasticity framework with an appropriate description of the surface stress effect.[27]

Increasing temperature can lower the strength because of thermal fluctuations in assisting dislocation nucleation. To understand the temperature and strain rate dependence of dislocation nucleation, Zhu et al.[28] have developed an atomistic model that integrates the reaction pathway calculation and transition-state-theory based analysis. Consider, as an example, surface dislocation nucleation in a Cu nanopillar under an applied constant strain rate. Because of the probabilistic nature of the thermally activated nucleation process, the nucleation stress has a distribution even if identical samples are used. The most probable nucleation stress is defined by the peak of the nucleation event frequency distribution. Based on this nucleation statistics-based definition, Zhu et al.[28] developed a non-linear theory to determine the nucleation stress as a function of temperature and strain rate. A key result is that the activation volume associated with the surface dislocation source is within $1b^3$–$10b^3$, much lower than that of bulk dislocation processes, $100b^3$–$1000b^3$. The physical effect

of such a small activation volume can be clearly seen from a linear version of the theory, giving an analytic formula of the nucleation stress,

$$\sigma = \sigma_a - \frac{k_B T}{\Omega} \ln \frac{k_B T N \nu_0}{E \dot{\varepsilon} \Omega}, \qquad (4)$$

where σ_a is the athermal stress of instantaneous nucleation and E is Young's modulus. Notice that the nucleation stress σ has a temperature scaling of $T \ln T$, and the activation volume Ω appears outside the logarithm so that the small Ω associated with a surface source should lead to sensitive temperature and strain rate dependence of nucleation stress, as quantitatively shown in atomistic simulations.[28] In very small volumes, surface dislocation nucleation is expected to dominate, as evidenced by the experiment.[29] As schematically shown in Figure 1, the strength mediated by surface nucleation should provide an upper bound to the size-strength relation in nanopillar compression experiments; this upper bound is strain rate sensitive because of the small activation volume.

Dislocation Exhaustion

What if mobile dislocations pre-exist in small volume materials? Under such conditions, ultra strength can be achieved by dislocation exhaustion. This has been experimentally measured in crystals of very small dimensions where the few dislocations present cannot multiply sufficiently before they are annihilated at free surfaces. Greer and Nix[16] measured the strength of Au pillars under uniaxial compression. For a pillar with a diameter as small as 300 nm, the compressive strength is increased to about 800 MPa, about 50 times higher than for bulk Au. Volkert et al.[17,30] have reported similar high strengths for both single crystal Au pillars and nanometer-sized ligaments in nanoporous Au. All of these experimental values are extremely high for Au, close to the theoretical predictions of ideal shear strength from *ab initio* calculations.[3]

Greer and Nix[16] have explained the ultra strength in Au nanopillars based on the concept of dislocation starvation. Unlike bulk samples, dislocations in nanopillars can travel only very small distances before annihilating at free surfaces, thereby reducing the overall dislocation multiplication rate. Gliding dislocations leave the crystal more rapidly than they multiply, decreasing the overall mobile dislocation density. Such processes would lead to a dislocation-starved state requiring very high stresses to nucleate new mobile dislocations.

Shan et al.[31] recently performed *in situ* compression experiments of submicrometer nickel pillars inside a transmission electron microscope (TEM). The experiments showed that the pillar structures contain a high density of initial defects after processing but can be made dislocation-free by applying purely mechanical stress. This phenomenon, termed mechanical annealing, provides evidence of source-limited deformation, where the hardening occurs through the progressive exhaustion of dislocation sources, causing dislocation starvation.

Dislocation-Interface Interaction

In thin films and layered materials, the strengthening arises from the constraints of the surrounding substrate and layers.[32] Achieving ultra strength requires that the film and layer thickness be in the range of a few to a few tens of nanometers. Under such conditions, the dislocation-interface interaction is expected to play an important role in controlling the strength.

The effect of layer thickness on flow strength has been summarized by Misra et al.[33] for metallic multilayers. They showed that a Hall-Petch–type model based on dislocation pile-up is applicable at the submicrometer length scales. At the few to a few tens of nanometers length scales, confined layer slip of single dislocations is the operative mechanism; the strength is influenced by interface stress and interface dislocation arrays. As layer thicknesses are further reduced to a few nanometers or less, the strength reaches a peak in ultra strength. This peak strength is set by the interface resistance to single dislocation transmission.

The dislocation-interface interactions may govern not only strength but also ductility. For example, Lu et al.[34] have reported experiments of an unusual combination of ultrahigh yield strength (~ 1 GPa) and high ductility (~ 14% elongation to failure) in ultrafine-grained copper (i.e., with a grain size of several hundred nanometers) containing layered nano-twins, typically tens of nanometers in thickness. While the ultrahigh strength can be attributed to the size-strengthening effect of thin twin lamellas, the mechanistic connection between the retained high ductility and twinned nanostructures is not fully understood.

In bulk nanocrystalline metals, tensile ductility is often limited by the onset of necking instability. This has been well studied at the continuum level. The central result is that the high strain rate sensitivity and the high rate of strain hardening can both help delay the onset and development of necking, thereby promoting tensile ductility.[35] To connect the phenomenological theories with nanostructure-mediated plastic deformation, one needs to first determine the rate-controlling mechanisms. The experiment by Lu et al.[36] showed that nano-twinned copper increases the rate sensitivity ($m \approx 0.02$) by up to an order of magnitude relative to microcrystalline metals with grain sizes in the micrometer range and a concomitant decrease in the activation volume by two orders of magnitude (e.g., down to $\Omega \approx 20b^3$ when twin lamellas are approximately 20 nm thick).

Zhu et al.[37] have studied the mechanistic origin of decreased activation volume and increased rate sensitivity in the nano-twinned system. They analyzed slip

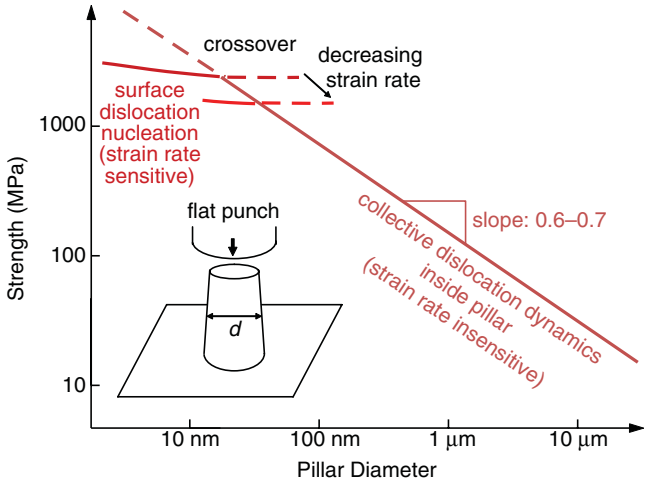

Figure 1. Illustration of the surface effect on the rate-controlling process and the size dependence of yield strength in micro- and nanopillars of diameter *d* under compression.[28]

transfer reactions between the lattice dislocation and coherent twin boundary (TB). Using the free-end nudged elastic band method, minimum energy paths were determined for reactions of absorption, desorption, and slip transmission. Predictions of yield stress, activation volume, and rate sensitivity were consistent with the experimental measurement. This agreement demonstrates that the slip transfer reactions at TBs are the rate-controlling mechanisms in nano-twinned copper.

Besides increasing the rate sensitivity, the dislocation-TB interaction causes an increase in the strain-hardening rate, which may play a key role in preserving the tensile ductility. The modeling study by Zhu et al.[37] indicated that in contrast to the general high angle grain boundaries in nanocrystals, which have a limited capacity of hardening, the coherent TB is quite hardenable as it gradually loses coherence during the initial stage of plastic deformation. This effective hardenability facilitates the accommodation of incompatible deformation between adjacent twins; it raises the resistance of plastic flow, promotes the strain hardening, and helps retain tensile ductility. Also, the coherent TB is more resistant to tensile decohesion compared to random boundaries and, therefore, can store larger amounts of deformation-induced incompatibility (interfacial dislocation content) before fracture occurs.

Intragrain to Intergrain Mechanisms

Nanocrystalline metals and alloys represent an important class of ultra-strength materials. They are single or multiphase polycrystals with nanoscale grain size (1–100 nm). Because of the increasing volume of grain boundary materials with decreasing grain size, the deformation in nanocrystals can be critically influenced by the grain boundary mediated mechanisms, which compete with the intragrain mechanisms such as the intersection of bulk dislocations. Here, we review two theoretical models on the transition from the intragrain to intergrain mechanisms; these models reveal the mechanistic underpinnings of grain size-dependent strength and activation volume.

The ultra-strength phenomenon in nanocrystals involves an interesting possibility for which size would be strongest. Specifically, the well-known Hall-Petch effect refers to the rise of plastic resistance with decreasing grain size. However, if the grain size drops into the nanometer range, a peak plastic resistance could result at a grain size of about 20 nm, leading to the breakdown of the Hall-Petch effect. Such effects have been observed by experiments and in computer simulations as well.[38]

Argon and Yip[39] developed an isostress model of the strongest size by focusing on the competition between grain boundary shear and near-boundary dislocation mechanism; here the shear of the grain boundary is considered to be similar to flow process in amorphous metals, constrained into a disordered layer of a thickness $\delta \sim b$. To a first approximation, they assumed both mechanisms were subject to the same applied stress but contributed to the overall strain rate in proportion to volume fractions. By realizing that the two processes operate close to respective athermal limits, Argon and Yip assumed both processes had an increased rate sensitivity, $m = 0.033$, and a correspondingly decreased activation volume compared to coarse-grained counterparts.

Figure 2 shows the modeling prediction of the strongest size as compared with computer simulations by molecular dynamics. According to the model, the breakdown of the Hall-Petch effect can be qualitatively understood as follows. At the large grain size, the near boundary dislocation mechanism dominates, and the strength increases with decreasing grain size by following the classic Hall-Petch relation. As the grain size reduces to the nanometer range, grain boundary shear gradually takes over as the dominant mechanism because of the increasing volume fraction of grain boundary materials. The strength then begins to decrease toward the athermal strength of grain boundary shear, which is lower than that of the near-boundary dislocation mechanism. Consequently, the competition between the two rate mechanisms leads to a peak strength.

In addition to the size-dependent strength, the activation volume also exhibits size dependence as experimentally measured in nanocrystalline and nano-twinned systems.[36,40] Conrad[40] and Armstrong and Rodriguez[41] developed isostrain models on the transition from the intra- to intergrain mechanisms to explain such size dependence. They considered two competing mechanisms that are in parallel to sustain the applied load: one involves the intragrain dislocation mechanism (e.g., intersection of forest dislocations, giving a large but size-independent activation volume typical of coarse-grained polycrystals); the other involves the near-boundary process (e.g., punching of a dislocation through a dense bundle of grain boundary dislocations, the emission of dislocations from grain boundaries, or the depinning of a propagating dislocation pinned by grain boundaries by impurities or ledges).[42,43] The size-dependence of activation volume is associated with the latter mechanism through a dislocation pile-up

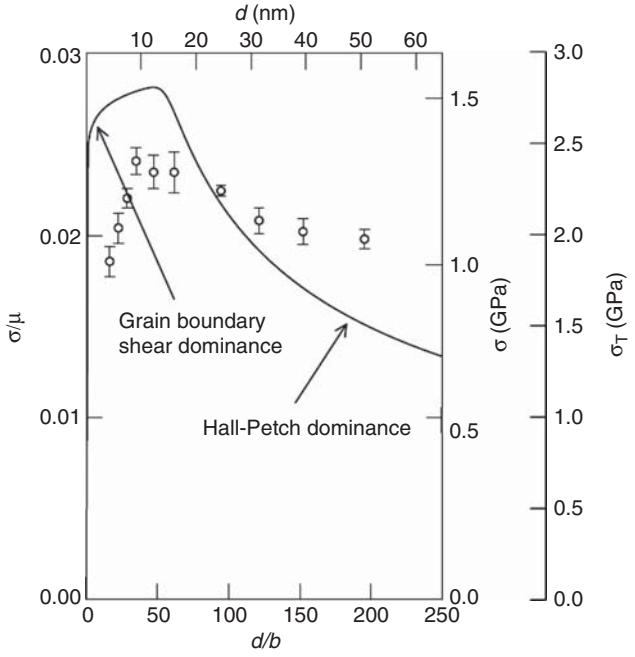

Figure 2. The strongest-size behavior for polycrystalline Cu from the Argon-Yip model[39] (solid line) and molecular dynamics simulations[38] (symbols), where d is the grain size, b is the magnitude of the Burgers vector, σ is the von Mises effective shear stress, σ_T is the tensile flow stress, μ is the shear modulus.

model. In Conrad's model, the total shear stress is taken as the sum of the shear resistances of the two mechanisms; this averaging scheme of the simple stress sum differs from the Argon-Yip model that involves the average strain rate based on volume fractions. As detailed in Reference 40, the size-dependent activation volume relation is derived as

$$\frac{1}{\Omega}=\frac{1}{\Omega_i}+\beta\,\frac{\mu b}{\sigma d}\,\frac{1}{\Omega_b}, \qquad (5)$$

where μ is the shear modulus, d is grain size, and β is a dimensionless number of order one. In Equation 5, Ω_i and Ω_b are the activation volumes of the intrinsic intragrain and intergrain mechanism, both of which are size-independent; the second term brings in the size-dependence through a dislocation pile-up model.

It is noteworthy that the foregoing models assume grain size is fixed in the course of plastic deformation. In contrast, abnormal grain growth has been observed in nanocrystals during plastic deformation at room to liquid-nitrogen temperatures.[44,45] This grain coarsening at low temperatures is largely driven by mechanical energy, as opposed to the thermally driven grain growth in coarse-grained samples at high temperatures. It has been attributed to the high-energy state of grain boundaries in nanocrystals.[46] Recent atomistic modeling has revealed the detailed atomic-level mechanisms of shear mediated grain boundary migration at the GPa-level high stresses.[47]

Deformation Twinning

In ultra-strength materials, the formation of deformation twins may dominate over dislocation slip. This has been observed by recent TEM experiments of nanocrystals.[42] The preference for deformation twinning in nanocrystals can be understood by comparing the critical resolved shear stress (CRSS) needed to emit a perfect dislocation, τ_f, with the CRSS required to initiate the partial twinning dislocation, τ_p, to generate stacking faults and deformation twins.[48] These CRSSs can be estimated by considering the energy balance between the elastic energy increase in expanding a boundary dislocation loop and the potential energy decrease associated with the work done by the CRSS. Assuming the source size is approximately equal to the grain size, d, the CRSSs for the emission of a perfect dislocation and twinning partials are given by $\tau_f/\mu = b/d$ and $\tau_p/\mu = b_p/d + \Gamma_{sf}$, respectively. Here, $\Gamma_{sf} = \gamma_{sf}/(\mu b_p)$, where γ_{sf} is the stacking fault energy, and b_p is the magnitude of the Burgers vectors of a partial dislocation. Equating τ_f and τ_p gives the critical grain size $d_c = (b - b_p)/\Gamma_{sf}$, where the transition will occur from the plastic response dominated by perfect dislocations for large grains to the twinning and stacking faults controlled plastic behavior for small grains. The estimated d_c is about 10 nm for aluminum nanocrystals.

It should be emphasized that the foregoing analysis of glide dislocations and deformation twins is based on the thermodynamic energy balance of expanding the existing boundary dislocations. As a result, their CRSSs only involve the material energetic parameter of stack fault energy, γ_{sf}, which characterizes the metastable stacking state of the lattice. Van Swygenhoven et al.[49] have emphasized the importance of examining the generalized stacking fault energy curve, which additionally provides activation-related parameters such as unstable stacking energy γ_{us} and unstable twinning energy γ_{ut}. Along this line, Asaro and Suresh[50] have performed the mechanics analysis of athermal emission of perfect dislocations and deformation twins from the grain boundary. The athermal stresses derived incorporate naturally γ_{us} and γ_{ut}. Finally, it is noteworthy that the thermal activation of deformation twins has not yet been studied for understanding the temperature and strain rate dependence of nucleation stresses at small length scales.

Fracture

Plastic flow and brittle fracture are competing deformation modes in ultra-strength materials. Bulk silicon is brittle, but silicon nanowires in tension can undergo large plastic deformation at room temperature.[51] A revealing analysis of brittle-ductile competition has been given by Dumitrica et al.[52] for a perfect single-walled carbon nanotube. By observing molecular dynamics simulations at various temperatures T and at short time scales (about 0.1 ns), they identified two primary mechanisms: the "cool" mechanism of brittle fracture at low T and the "hot" mechanism of formation of Stone-Wales defects (i.e., dislocation dipoles) at high T. To explore the competition at long time scales, they have studied the energy landscapes governing the two processes. They found the brittle mode of bond breaking requires little thermal agitation; the fracture stress is controlled by the ideal tensile strength of the C-C bond. In contrast, the Stone-Wales defect formation by single bond rotation sensitively depends on temperature, implying a small activation volume associated with this process. According to transition state theory, the activation energy under constant stress needs to be reduced to $Q = k_B T \ln(N\nu t)$ in order to observe the formation of Stone-Wales dipole over the test duration t (probability ~ 1). Dumitrica et al. have further calculated Q as a function of stress. Then, the stress needed to form the Stone-Wales dislocation dipole at different temperatures and times can be backed out from the formula of Q given previously. Figure 3 shows the predicted breaking-strain map. Such a mechanism map is expected to provide useful guidance for the experimental study of temperature and strain rate dependence of mechanical responses of carbon nanotubes.

The foregoing analysis has considered an idealized situation of competition between the brittle and ductile response in a perfect system.[52–54] In an alternative scenario, such competition could occur at the crack tip in a system with a pre-existing crack.[55] In this case, bond breaking at the

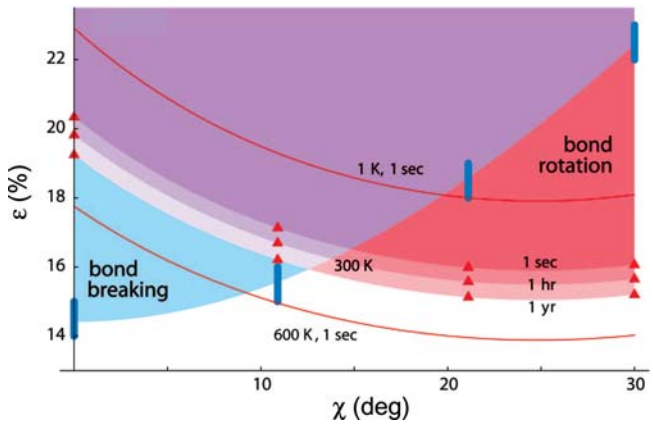

Figure 3. Breaking-strain (ε) map for carbon nanotubes of different chiralities (χ) at various load durations and temperatures.[52]

crack tip may have different temperature and strain rate dependences. The analysis along the line of Dumitrica et al.[52] needs to be performed to better understand the brittle-to-ductile transition in ultra-strength materials.

Conclusions

In the past decade, we have seen a dramatic increase in experimental studies of ultra-strength materials and phenomena, driven by technological demands and projections. The high strength achieved often is caused by a scarcity of grown-in defects and the exhaustion of mobile defect population destabilized by close proximity to interfaces or surfaces, which consequently cause the strength to be defect nucleation controlled rather than propagation controlled. The plastic deformation in the ultra-strength regime is generally characterized by enhanced strain rate sensitivity and temperature sensitivity. Mechanisms of strain hardening (or the lack thereof), interfacial structural evolution and decohesion, and tensile ductility are some of the issues that need to be further considered for comprehensive understanding of ultra-strength materials at low temperatures. Although temperature-controlled nanomechanical testing is still quite rare today, it is a direction for future growth. From a theoretical standpoint, we expect ultrahigh stress will have a significant impact on diffusive and hybrid displacive-diffusive processes as well. Boundaries of the deformation mechanism map[56] in the parametric space of stress, temperature, and strain rate can be expected to shift significantly compared to those of coarse-grained materials,[57–59] thereby allowing exploration of crossover behavior that can provide new understanding of the deformation kinetics of ultra-strength materials.[60]

Acknowledgments

TZ would like to thank support by NSF CMMI-0653769, 0758265, 0758554, 0825435. JL would like to thank support by NSF CMMI-0728069, AFOSR, ONR N00014-05-1-0504, and Ohio Supercomputer Center.

References

1. L.B. Freund, S. Suresh, *"Thin Film Materials: Stress, Defect Formation and Surface Evolution"* (Cambridge University Press, Cambridge, UK, 2003).
2. S. Ogata, J. Li, S. Yip, *Science* **298**, 807 (2002).
3. S. Ogata, J. Li, N. Hirosaki, Y. Shibutani, S. Yip, *Phys. Rev. B* **70**, 104104 (2004).
4. T. Li, J.W. Morris, N. Nagasako, S. Kuramoto, D.C. Chrzan, *Phys. Rev. Lett*. **98**, 105503 (2007).
5. C.A. Schuh, T.C. Hufnagel, U. Ramamurty, *Acta Mater*. **55**, 4067 (2007).
6. J. Li, *MRS Bull*. **32**, 151 (2007).
7. M.A. Meyers, A. Mishra, D.J. Benson, *Prog. Mater. Sci*. **51**, 427 (2006).
8. M.R. Falvo, G.J. Clary, R.M. Taylor, V. Chi, F.P. Brooks, S. Washburn, R. Superfine, *Nature* **389**, 582 (1997).
9. M.F. Yu, B.S. Files, S. Arepalli, R.S. Ruoff, *Phys. Rev. Lett*. **84**, 5552 (2000).
10. B. Peng, M. Mocascio, P. Zapol, S. Li, S.L. Mielke, G.C. Schatz, H.D. Espinosa, *Nat. Nanotechnol*. **3**, 626 (2008).
11. I. Kaplan-Ashiri, S.R. Cohen, K. Gartsman, V. Ivanovskaya, T. Heine, G. Seifert, I. Wiesel, H.D. Wagner, R. Tenne, *Proc. Nat. Acad. Sci. U.S.A*. **103**, 523 (2006).
12. B. Wen, J.E. Sader, J.J. Boland, *Phys. Rev. Lett*. **101**, 175502 (2008).
13. S. Hoffmann, I. Utke, B. Moser, J. Michler, S.H. Christiansen, V. Schmidt, S. Senz, P. Werner, U. Gosele, C. Ballif, *Nano Lett*. **6**, 622 (2006).
14. B. Wu, A. Heidelberg, J.J. Boland, J.E. Sader, X.M. Sun, Y.D. Li, *Nano Lett*. **6**, 468 (2006).
15. B. Wu, A. Heidelberg, J.J. Boland, *Nat. Mater*. **4**, 525 (2005).
16. J.R. Greer, W.D. Nix, *Phys. Rev. B* **73**, 245410 (2006).
17. C.A. Volkert, E.T. Lilleodden, *Philos. Mag*. **86**, 5567 (2006).
18. W.W. Gerberich, W.M. Mook, C.R. Perrey, C.B. Carter, M.I. Baskes, R. Mukherjee, A. Gidwani, J. Heberlein, P.H. McMurry, S.L. Girshick, *J. Mech. Phys. Solids* **51**, 979 (2003).
19. Z.W. Shan, G. Adesso, A. Cabot, M.P. Sherburne, S.A. Syed Asif, O.L. Warren, D.C. Chrzan, A.M. Minor, A.P. Alivisatos, *Nat. Mater*. **7**, 947 (2008).
20. C. Lee, X.D. Wei, J.W. Kysar, J. Hone, *Science* **321**, 385 (2008).
21. G.H. Vineyard, *J. Phys. Chem. Solids* **3**, 121 (1957).
22. G. Henkelman, B.P. Uberuaga, H. Jonsson, *J. Chem. Phys*. **113**, 9901 (2000).
23. A. Gouldstone, K.J. Van Vliet, S. Suresh, *Nature* **411**, 656 (2001).
24. P. Schall, I. Cohen, D.A. Weitz, F. Spaepen, *Nature* **440**, 319 (2006).
25. J. Li, K.J. Van Vliet, T. Zhu, S. Yip, S. Suresh, *Nature* **418**, 307 (2002).
26. R. Hill, *Math. Proc. Cambridge Philos. Soc*. **77**, 225 (1975).
27. H.S. Park, P.A. Klein, *Phys. Rev. B* **75**, 085408 (2007).
28. T. Zhu, J. Li, A. Samanta, A. Leach, K. Gall, *Phys. Rev. Lett*. **100**, 025502 (2008).
29. H. Bei, Y.F. Gao, S. Shim, E.P. George, G.M. Pharr, *Phys. Rev. B* **77**, 060103 (2008).
30. C.A. Volkert, E.T. Lilleodden, D. Kramer, J. Weissmuller, *Appl. Phys. Lett*. **89**, 061920 (2006).
31. Z.W. Shan, R.K. Mishra, S.A.S. Asif, O.L. Warren, A.M. Minor, *Nat. Mater*. **7**, 115 (2008).
32. O. Kraft, L.B. Freund, R. Phillips, E. Arzt, *MRS Bull*. **27**, 30 (2002).
33. A. Misra, J.P. Hirth, R.G. Hoagland, *Acta Mater*. **53**, 4817 (2005).
34. L. Lu, Y.F. Shen, X.H. Chen, L.H. Qian, K. Lu, *Science* **304**, 422 (2004).
35. E. W. Hart, *Acta Metall*. **15**, 351 (1967).
36. L. Lu, R. Schwaiger, Z.W. Shan, M. Dao, K. Lu, S. Suresh, *Acta Mater*. **53**, 2169 (2005).
37. T. Zhu, J. Li, A. Samanta, H.G. Kim, S. Suresh, *Proc. Nat. Acad. Sci. U.S.A*. **104**, 3031 (2007).
38. J. Schiotz, K.W. Jacobsen, *Science* **301**, 1357 (2003).
39. A.S. Argon, S. Yip, *Philos. Mag. Lett*. **86**, 713 (2006).
40. H. Conrad, *Nanotechnology* **18**, 325701 (2007).
41. R.W. Armstrong, P. Rodriguez, *Philos. Mag*. **86**, 5787 (2006).
42. M. Dao, L. Lu, R.J. Asaro, J.T.M. De Hosson, E. Ma, *Acta Mater*. **55**, 4041 (2007).
43. H. Van Swygenhoven, P.M. Derlet, A.G. Froseth, *Acta Mater*. **54**, 1975 (2006).
44. K. Zhang, J.R. Weertman, J.A. Eastman, *Appl. Phys. Lett*. **87**, 061921 (2005).
45. D.S. Gianola, S. Van Petegem, M. Legros, S. Brandstetter, H. Van Swygenhoven, K.J. Hemker, *Acta Mater*. **54**, 2253 (2006).
46. J.C.M. Li, *Phys. Rev. Lett*. **96**, 215506 (2006).
47. J.W. Cahn, Y. Mishin, A. Suzuki, *Acta Mater*. **54**, 4953 (2006).
48. M.W. Chen, E. Ma, K.J. Hemker, H.W. Sheng, Y.M. Wang, X.M. Cheng, *Science* **300**, 1275 (2003).
49. H. Van Swygenhoven, P.M. Derlet, A.G. Froseth, *Nat. Mater*. **3**, 399 (2004).
50. R.J. Asaro, S. Suresh, *Acta Mater*. **53**, 3369 (2005).
51. X.D. Han, K. Zheng, Y.F. Zhang, X.N. Zhang, Z. Zhang, Z.L. Wang, *Adv. Mater*. **19**, 2112 (2007).
52. T. Dumitrica, M. Hua, B.I. Yakobson, *Proc. Nat. Acad. Sci. U.S.A*. **103**, 6105 (2006).
53. K. Kang, W. Cai, *Philos. Mag*. **87**, 2169 (2007).
54. T. Belytschko, S.P. Xiao, G.C. Schatz, R.S. Ruoff, *Phys. Rev. B* **65**, 235430 (2002).
55. D.H. Warner, W.A. Curtin, S. Qu, *Nat. Mater*. **6**, 876 (2007).
56. H.J. Frost, M.F. Ashby, *"Deformation-Mechanism Maps"* (Pergamon Press, New York, 1982).
57. V. Yamakov, D. Wolf, S.R. Phillpot, A.K. Mukherjee, H. Gleiter, *Nat. Mater*. **3**, 43 (2004).
58. S. Yip, *Nat. Mater*. **3**, 11 (2004).
59. D.L. McDowell, *Mater. Sci. Eng., R* **62**, 67 (2008).
60. S. Suresh, J. Li, *Nature* **456**, 716 (2008). □

Dynamic Material Analysis

MDC Precision Motion Control Vacuum Equipment for Materials Research Applications

Visit us online or Call for a Free Catalog

Advanced Sample Manipulation System

Transferable Experimental Station easily engages with interior mounted receiver

Precision Magnetic Transporters with independent rotary and linear motion

MDC's high coupling precision magnetic transporters handle more axial force and torque and exhibit better compliance and load carrying capability than typically expected from a magnetically-coupled feedthrough. Together with our Transferable Experimental Stations they provide dependable solutions to precise manipulation of sample stages requiring very good tactical feedback and high duty cycling.

1000's of Components in-stock & ready to ship-today!

Custom Engineering Available

Insulator Seal, a division of MDC Vacuum Products, provides UHV-grade electrical feedthroughs and optical viewports for Ceramic-Metal seal applications including instrumentation applications such as Spectroscopy, Electron microscopy, Surface analysis and Semiconductor process controls.

ISO 9001:2000

USB 2.0 Instrumentation

ISI introduces the Industry's 1st hermetic USB feedthrough that allows for the user to connect a feedthrough directly to a computer with a high speed 2.0 USB connection port.

Micro Midgy Feedthrough

A Full 12 kV rating, in a ceramic under an inch in length, is achieved by utilizing ISI's air-exclusion, air-side connector.

For feedthroughs call ISI at (800) 548-9509 or visit www.insulatorseal.com

MDC VACUUM PRODUCTS, LLC

mdcvacuum.com
1-800-443-8817